



Computation of hemodynamics in the left coronary artery with variable angulations

Thanapong Chaichana^a, Zhonghua Sun^{a,*}, James Jewkes^b

^a Discipline of Medical Imaging, Department of Imaging and Applied Physics, Curtin University, G.P.O Box U1987, Perth, Western Australia 6845, Australia

^b Fluid Dynamics Research Group, Department of Mechanical Engineering, Curtin University, Perth, Western Australia 6845, Australia

ARTICLE INFO

Article history:

Accepted 16 April 2011

Keywords:

Coronary artery disease
Angulation
Computational fluid dynamics
Wall shear stress
Wall shear stress gradient

ABSTRACT

The purpose of this study was to investigate the hemodynamic effect of variations in the angulations of the left coronary artery, based on simulated and realistic coronary artery models. Twelve models consisting of four realistic and eight simulated coronary artery geometries were generated with the inclusion of left main stem, left anterior descending and left circumflex branches. The simulated models included various coronary artery angulations, namely, 15°, 30°, 45°, 60°, 75°, 90°, 105° and 120°. The realistic coronary angulations were based on selected patient's data with angles ranging from narrow angles of 58° and 73° to wide angles of 110° and 120°. Computational fluid dynamics analysis was performed to simulate realistic physiological conditions that reflect the *in vivo* cardiac hemodynamics. The wall shear stress, wall shear stress gradient, velocity flow patterns and wall pressure were measured in simulated and realistic models during the cardiac cycle. Our results showed that a disturbed flow pattern was observed in models with wider angulations, and wall pressure was found to reduce when the flow changed from the left main stem to the bifurcated regions, based on simulated and realistic models. A low wall shear stress gradient was demonstrated at left bifurcations with wide angles. There is a direct correlation between coronary angulations and subsequent hemodynamic changes, based on realistic and simulated models. Further studies based on patients with different severities of coronary artery disease are required to verify our results.

© 2011 Elsevier Ltd. All rights reserved.

1. Introduction

Atherosclerosis is the leading cause of morbidity and mortality in the advanced countries. The causes of atherosclerosis are multifactorial and identification of these factors could allow earlier detection and prevention of the disease. Hemodynamics and vessel geometry may play an important role in the cause of plaque formation, since atherosclerotic plaques occur frequently in well-recognized arterial regions of curvature, bifurcated area and vessel branches (Zarins et al., 1983; Asakura and Karino, 1990; Conner, 1994). Blood flow variations, particularly those related to the rate of change of stream-wise velocity perpendicular to the blood vessel wall (known as the wall shear stress), have been reported to be related to the pathogenesis of atherosclerosis (Lehoux, 2006; Sabbah et al., 1986).

Early hemodynamic analysis of coronary artery disease performed using computational fluid dynamic (CFD) techniques has been typically performed using one of two approaches, they were based on either simulated models or realistic coronary artery geometry simulations (Lim and Kern, 2005; Katritsis et al., 2007;

Shanmugavelayudam et al., 2010; Wellnhofer et al., 2010; Nordgaard et al., 2010). As far as we know, no systematic studies have been performed hitherto that relate bifurcation angles to flow instabilities predisposing to the formation of atherosclerotic lesions. The left coronary artery differs from the right coronary artery in terms of geometric appearance as the left side has a very short main stem, which quickly divides into left anterior descending and left circumflex with an angle formed between these two branches. Thus the angulation between these two coronary branches induces local hemodynamic changes, which may pose a potential risk for development of atherosclerosis. The aim of this study was to investigate the relationship between hemodynamics and angulations at the left coronary artery, based on simulated models and realistic patients' data. Various angles were simulated at the left coronary artery with the aim of identifying the effect of angulation on the subsequent hemodynamic changes to the left coronary artery.

2. Materials and Methods

2.1. Measurement of left coronary artery anatomical details

Four patients suspected of coronary artery disease underwent multislice CT angiography and were included in the patient datasets. This original DICOM

* Corresponding author. Tel.: +61 8 9266 7509; fax: +61 8 9266 2377.
E-mail address: z.sun@curtin.edu.au (Z. Sun).

(digital imaging and communication in medicine) data was transferred to a separate workstation equipped with Analyze version 7.0 (Analyze Direct, Inc., Lexana, KS, USA) for image post-processing and segmentation. Three-dimensional (3D) volume data was post-processed and segmented using a semi-automatic method with a CT number thresholding technique (Sun et al., 2003, 2004) and manual editing was performed in some slices to remove soft tissues and artifacts. Four models were produced with a special focus on the left coronary artery (LCA) and its branches. The 3D LCA models were saved in ‘STL’ stereolithography CAD format for further reconstruction purposes. Anatomic measurements were performed at the LCA location and its branches in the volumetric models so that these measurements could be used to provide suitable dimensions for the simulated LCA models, as shown in Table 1. Fig. 1 shows anatomical details of the LCA with an angle formed between the left anterior descending (LAD) and left circumflex (LCx) branches.

This investigation conforms to the principles outlined in the declaration of Helsinki for use of human subjects (World Medical Association declaration of Helsinki, 1997). Since patients underwent routine CT scanning for clinical diagnosis of coronary artery disease, and only the DICOM images were used for generation of 3D coronary artery images, with patient’s details being de-identified, there is no ethical issue involved in this study.

2.2. Generation of simulated left coronary artery models

The geometry of a simulated, perpendicular (90°) model was generated based on the anatomical details of LCA and standard dimensions measured based on Fig. 1, using Blender version 2.48 (Blender Institute, Amsterdam, Netherlands). The surface of the 90° LCA model was used as a reference model, which was then converted into a solid model. A bifurcation angle of 80° is recommended as a cut off value to determine whether there is presence of coronary artery disease, as confirmed by previous reports studying the natural distribution of coronary

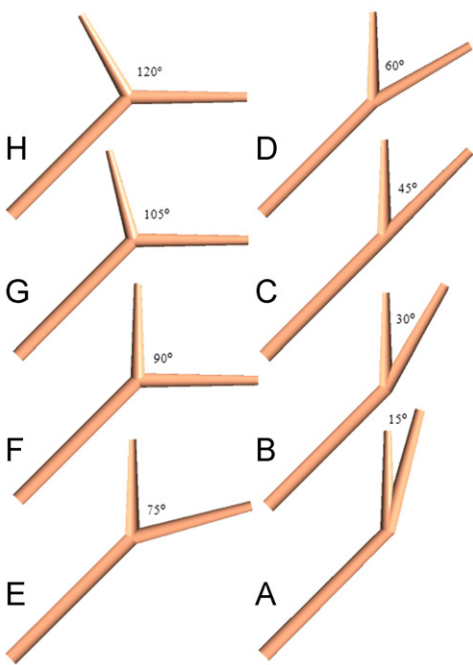


Fig. 2. Diagrams showing variable angles of the left coronary artery, including 120°, 105°, 90°, 75°, 60°, 45°, 30° and 15°.

Table 1
Measurements of anatomical dimensions at the left coronary model.

Diameter of LCA (mm)	Distance between bifurcation to proximal/distal segment (mm)
LMS 3.0	Proximal inlet of LMS 35
LAD 2.0	Distal outlet of LAD 25
LCx 1.5	Distal outlet of LCx 20

LMS—left main stem, LAD—left anterior descending, LCx—left circumflex.

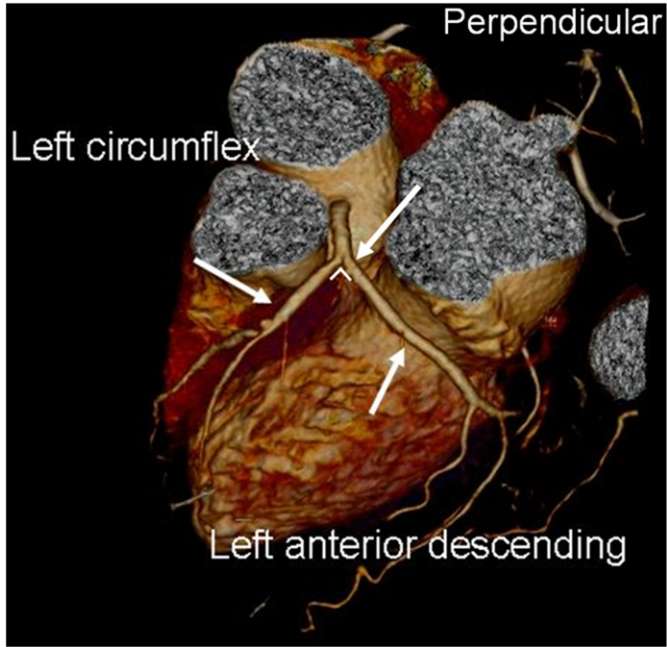


Fig. 1. 3D CT visualization of a normal left coronary artery with side branches in a patient with suspected coronary artery disease.

bifurcation angles (Reig and Petit, 2004; Pfleiderer et al., 2006). Our simulation on different angles of the left coronary artery reflects the range of angulations from very small to large angles, which enables us to perform an in-depth study of the relationship between angulation and development of atherosclerosis. Based on the reference model, seven other models were generated by changing the angle between LAD and LCx these included 15°, 30°, 45°, 60°, 75°, 105° and 120°. All baseline models were saved in ‘STL format’ for producing mesh models. Fig. 2 shows variable angles that were simulated in the left coronary artery models. Finally the merging of side branches within left main trunk generated sharp edges at the bifurcation regions, which could potentially have an undesirable impact on local flow simulation (He and Ku, 1995). Therefore, gentle B-spline smoothing was applied at the interface between branches and the trunk to reduce any potential non-physical behavior that could be induced by sharp edges. The splitting of flow rate at a symmetric bifurcation is defined by Zheng et al. (2006) and Lou and Yang (1993). Their flow rate system of equal diameter branches can be defined as a splitting ratio (Zheng et al., 2006):

$$Q_{LMS} = Q_{LCx} + Q_{LAD} \tag{1}$$

$$R_s = \frac{Q_{LCx}}{Q_{LAD}} \tag{2}$$

where $Q_{LMS} = \pi r_{LMS}^2 \vec{V}_{LMS}$ is the flow rate in parent with r_{LMS}^2 and \vec{V}_{LMS} being radius and velocity at main trunk, respectively, Q_{LCx} and Q_{LAD} are the flow rates in daughter branches. However, in this study, the two left coronary artery branches are unequal in diameter and distance in regard to the main left coronary artery, as shown in Table 1. In our case, R_s (splitting ratio) of a 90° model is calculated as $R_s = (\pi r_{LCx}^2 \vec{V}_{LCx}) / (\pi r_{LAD}^2 \vec{V}_{LAD}) = 9 \vec{V}_{LCx} / 16 \vec{V}_{LAD}$.

2.3. Generation of realistic left coronary artery models

The patient 3D LCA models consisting of the ascending aorta, and right and left coronary arteries were then imported into a computer-aided design program using Blender version 2.48. Four volume models were reconstructed into the surface models, which were then converted into solid models and saved in ‘STL format’ for generation of CFD mesh models. Fig. 3 shows four sample realistic patient left coronary models with variable angulations. The realistic patient bifurcation angles ranged from 58° to 73°, 110° and 120°, respectively. These patients were selected to reflect the relationship between hemodynamics and angulations in the LCA. In summary, there were a total of twelve models consisting of four patient models and eight simulated models.

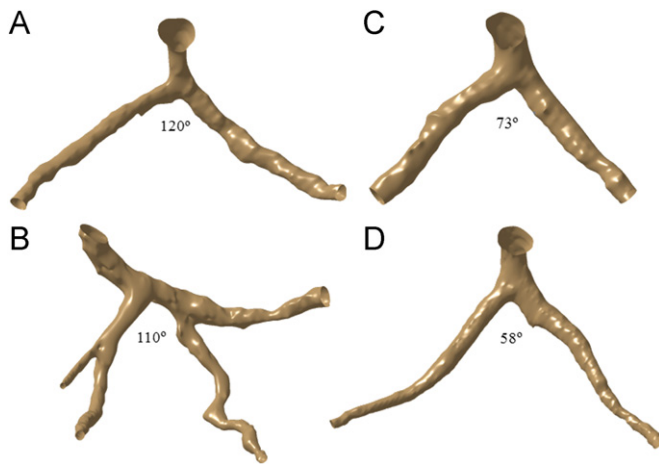


Fig. 3. Realistic coronary models in 4 selected patients with different angles at the left coronary artery including 120°, 110°, 73° and 58°.

Table 2

Details of Hex-meshing for both simulated and realistic models.

Angulations (deg.)	No. of nodes	No. of cells
<i>Simulated left coronary models</i>		
120	326,325	365,517
105	353,589	369,218
90	336,807	354,827
75	343,290	357,502
60	358,395	366,925
45	343,626	364,552
30	340,923	358,038
15	320,460	330,427
<i>Realistic left coronary models</i>		
120	327,465	363,519
110	346,659	361,150
73	337,872	351,996
58	334,167	353,215

2.4. CFD simulation in the left coronary artery—generation of meshes

All of the above models were used to create hexahedral meshes with which to perform the CFD simulations (mesh details are shown in Table 2). The meshes were generated using ANSYS ICEM CFD version 12 (ANSYS, Inc., Canonsburg, PA, USA), with details having been described in previous studies (Sun and Chaichana, 2010, 2009). Finally, the twelve 3D meshes were saved in 'GTM format' for CFD computation.

2.5. Application of physiological parameters

In order to ensure that our analysis reflects the realistic simulation of *in vivo* conditions, realistic physiological boundary conditions were applied for 3D numerical analysis. The transient simulation was performed using accurate hemodynamic rheological and material properties, as described in a previous study (Frauenfelder et al., 2006). Fig. 4 shows the pulsatile flow rates and pressure (Nichols and O'Rourke, 2005) at the aorta and LCA, reconstructed using a Fourier series (Smith, 1997) in Matlab (Math Works, Inc. Natick, MA, USA). This Fourier series was applied using ANSYS CFX Command Language (CCL) programming to define velocity and pressure boundary conditions. Pulsatile velocity was applied as an inlet boundary condition at the left main stem, and pulsatile pressure was applied at the left anterior descending and left circumflex outlet boundaries. Appropriate rheological parameters were applied with a blood density of 1060 kg/m³ and blood viscosity of 0.0035 Pa s (Boutsianis et al., 2004; Milnor, 1989). The blood flow was assumed to be laminar and a no-slip condition was applied at the walls. Blood was assumed to be a Newtonian and incompressible fluid (Johnston et al., 2004, 2006; Borghi et al., 2008).

2.6. Performance of CFD computation

The Navier–Stokes equations were solved using the ANSYS CFX CFD package (version 12—ANSYS, Inc.), on a Microsoft Windows XP 32-bit machine, 4 MB RAM

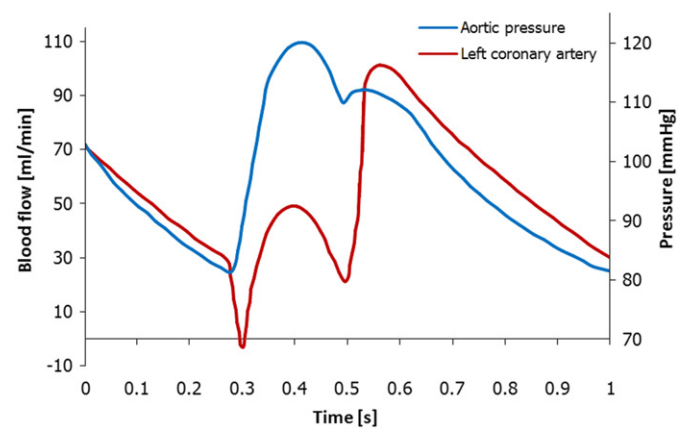


Fig. 4. Cardiac pulsatile velocity and pressure are applied for computational fluid dynamic simulation at the left coronary artery.

with a dual core 2.4 GHz CPU. The CFD simulation was run for 80 time-steps, representing 1.0 s of pulsatile flow (0.0125 s per time step), with each time step converged to a residual target of less than 1×10^{-4} by approximately 100 iterations. The CFD solution was fully converged by approximately 8000 time iterations per LCA model. The calculation time for each LCA model was approximately 5 h. The configuration of this simulation is similar to those in previously published simulations (Sun and Chaichana, 2010, 2009). Flow patterns, flow velocity, wall pressure, wall shear stress (WSS) and wall shear stress gradient (WSSG) were calculated and visualized using ANSYS CFD-Post version 12 (ANSYS, Inc.). The parameter used to characterize the impact of bifurcation angle on hemodynamic flow was calculated as the magnitude of local wall shear stress gradient (Kleinstreuer et al., 2001), which is defined as

$$\text{WSSG} = \sqrt{\left(\frac{\partial \tau_{w,m}}{\partial m}\right)^2 + \left(\frac{\partial \tau_{w,n}}{\partial n}\right)^2} \quad (3)$$

where m is the temporal mean WSS direction, n is tangential to the surface and normal to m , $\tau_{w,m}$ and $\tau_{w,n}$ are WSS components along m and n directions, respectively and $\partial \tau_{w,m}/\partial m$ and $\partial \tau_{w,n}/\partial n$ are the off-diagonal components of $\nabla \tau_w$ tensor, which is obtained by computing a spatial derivative of WSS vector with respect to the Cartesian coordinates (x, y, z directions). The local WSS is calculated as $\tau_w = \mu(\partial \vec{v}_t / \partial y)$, where μ is blood viscosity, $\partial \vec{v}_t$ is velocity near wall perpendicular to surface and ∂y is distance to the wall surface. The WSSG components demonstrated that localized cellular proliferation may coincide with sudden pronounced changes in WSS (LaDisa et al., 2004; Ojha, 1993; White et al., 2001; Lei et al., 2001). Therefore the temporal WSSG is an alteration of WSS over a small period of time at the same location (White et al., 2001; Ojha, 1993), and can be obtained by taking the time derivative of the local WSSG, which is considered as $\partial \tau_w / \partial t$ and this has been described before (Lei et al., 1996). The time-dependent alterations in WSS and temporal WSSG were determined to evaluate the impact of bifurcation angles upon the flow and the ANSYS CCL language was used to develop a code to compute WSSG in ANSYS CFX-Post processing.

3. Results

The simulated and realistic left coronary artery models were successfully performed with CFD analysis under the *in vivo* physiological conditions during the systolic and diastolic phases. The analysis demonstrates a strong relationship between hemodynamics and angulations at the left coronary artery, as observed in both types of models.

3.1. Simulated left coronary artery models

Peak systolic velocity and pressure were reached at a time of 0.4 s during the cardiac cycles. Velocity patterns measured with different angulations of the simulated models are shown in Fig. 5. The CFD analysis showed that a small region of low-velocity blood flow distributed in the small-angled models gradually became a large region of flow separation when the angulations were

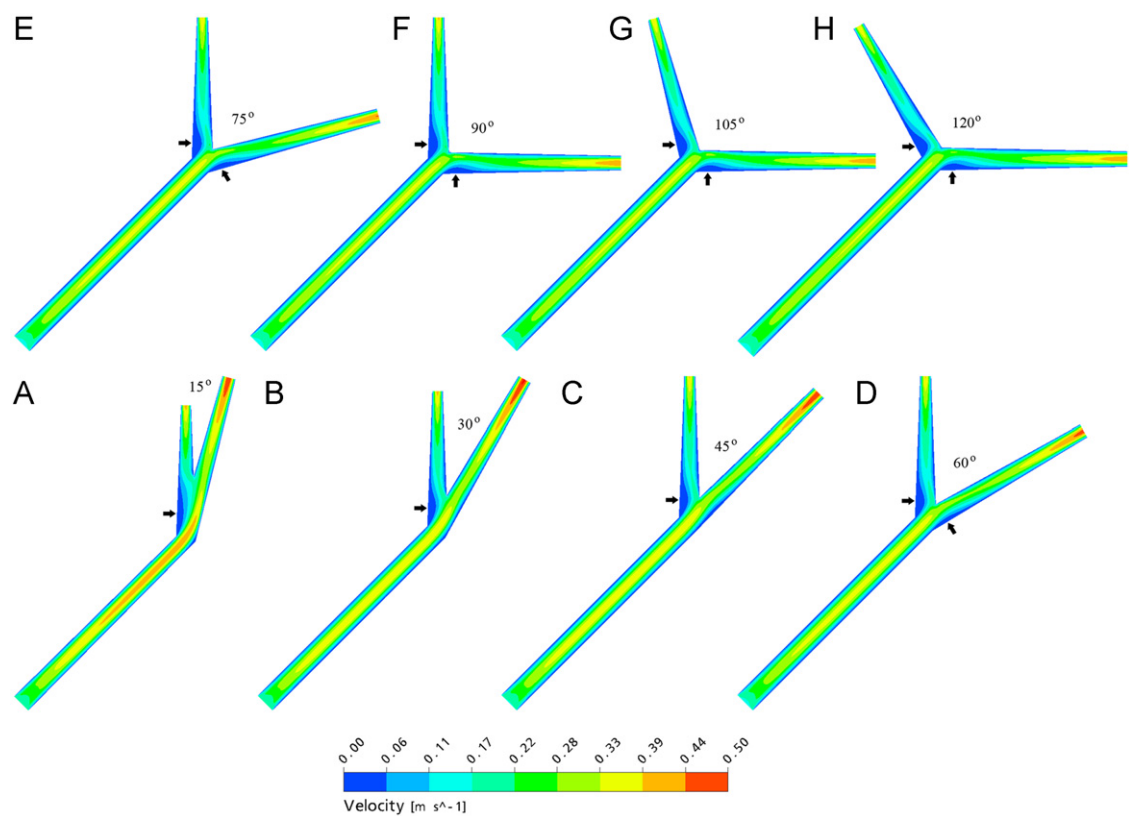


Fig. 5. Velocity observed with variable angles of the simulated left coronary artery models generated at peak systolic phase of 0.4 s. Arrows show the distribution regions of low flow and a big region of flow separation present in the wide-angled models.

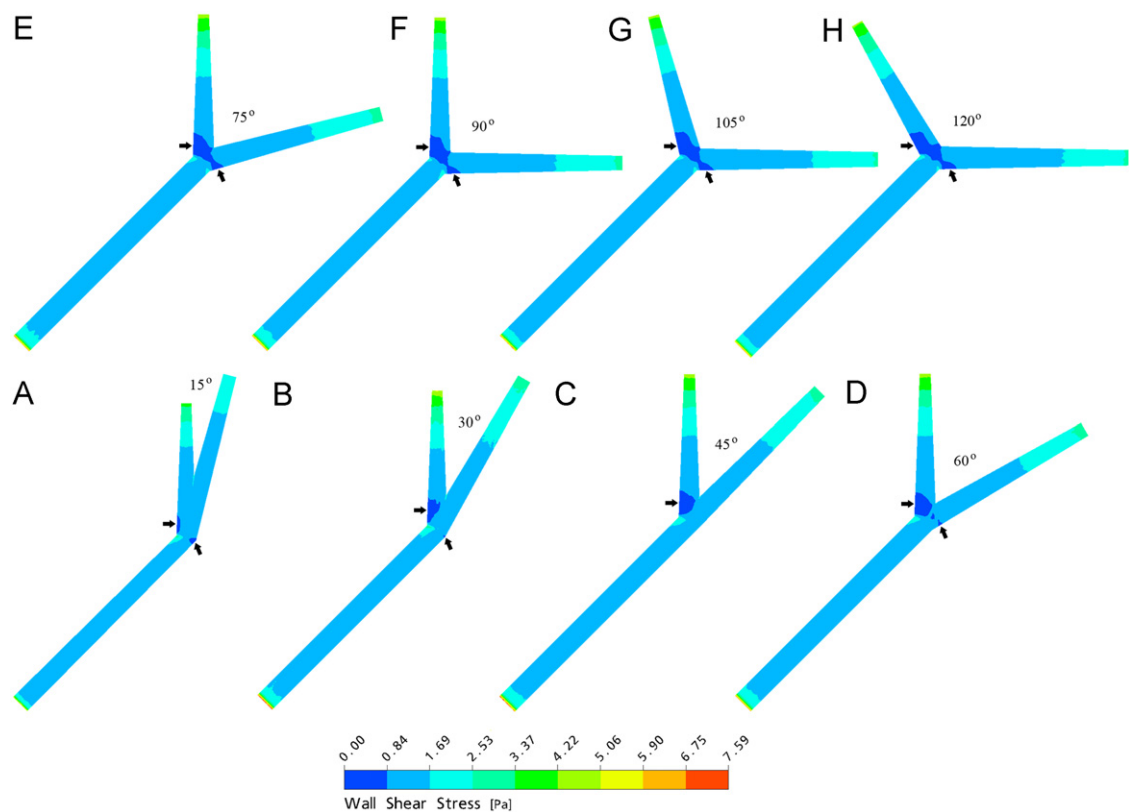


Fig. 6. Wall shear stress observed with variable angles of the simulated left coronary artery models generated at peak systolic phase of 0.4 . Arrows present the low wall shear stress distributions and a big region of low wall shear stress distributed in the wide coronary bifurcation.

increased, and this is particularly apparent at the location of the left coronary bifurcation.

Low WSS regions occurred at bifurcations where the left coronary main stem branches into left anterior descending and left circumflex. Fig. 6 demonstrates that WSS regions were found to reduce in wide-angled models when compared to the narrowed models and this phenomenon is particularly obvious in the systolic phase.

Similarly, wall pressure was affected to some extent with the change of angulations in different models. Fig. 7 displays that wall pressure increased from narrow-angled models to wide-angled models, particularly near the left coronary bifurcation. This is especially obvious in the model with a 15° angulation, as the results show significantly reduced wall pressure when the blood flows through from the left main stem to the left anterior descending and left circumflex branches.

Fig. 8 presents the magnitude of temporal WSSG and the regions of low WSSG at the left coronary bifurcations. A very low WSSG occurred in models with an angle of 120°, 105°, 90° and 75°, with the measured values ranging from 15.76 to 219.82 kg/m² s². In contrast, low temporal WSSG was not significantly apparent in small angle models such as 15° and 30° models. The temporal WSSG magnitude ranging 423.89–627.95 and 627.95–832.02 kg/m² s² was only measured in the models with an angle of 15°, 30°, 45°, 60°.

3.2. Realistic left coronary artery models

The analysis of realistic models is consistent with which was observed in the simulated models, showing a direct correlation between hemodynamic effects and the angulation of left coronary models. Fig. 9 demonstrates that flow velocity was decreased at

bifurcation regions, and a small low-velocity region was observed in the small-angled models, becoming a large separated region in the wide-angled models.

WSS was found to be related to blood flow velocity at bifurcating regions. Low WSS was noticed in the bifurcated locations (angles between both left main artery branches and side branches), as shown in Fig. 10. The realistic coronary artery shapes introduced complex wall geometry that directly affected the WSS and wall pressure. However, our analysis showed that the impact on low WSS distributions at the left bifurcation was largely in wide-angled models, and this reflects our similar observations in the simulated models (shown in Fig. 6).

Similarly, wall pressure was noticed to change with different angulations of realistic left coronary models. Wall pressure decreased from wide-angled models to narrow-angled models. This is particularly apparent in the model with a 73° angulation when compared to a 120° angulation, as shown in Fig. 11. Again, this is consistent with that observed in the simulated models.

The magnitude of temporal WSSG is shown in Fig. 12. The regions of low WSSG were distributed around the left coronary bifurcations. The magnitude of low WSSG was obviously demonstrated for bifurcations with 120° and 110° angulations, with measured WSSG values ranging from 15.76 to 219.82 kg/m² s². Low WSSG also occurred at 58° angulation model due to the complex shape of the daughter branches. This indicates the difference between realistic models and simulated models as the realistic models represent the patient's actual arterial geometry, while simulated models do not reflect the complex wall geometry such as curved or tortuous appearance of the vessel wall. The temporal WSSG magnitude between 627.95 and 832.02 kg/m² s² was measured only in the 58° model.

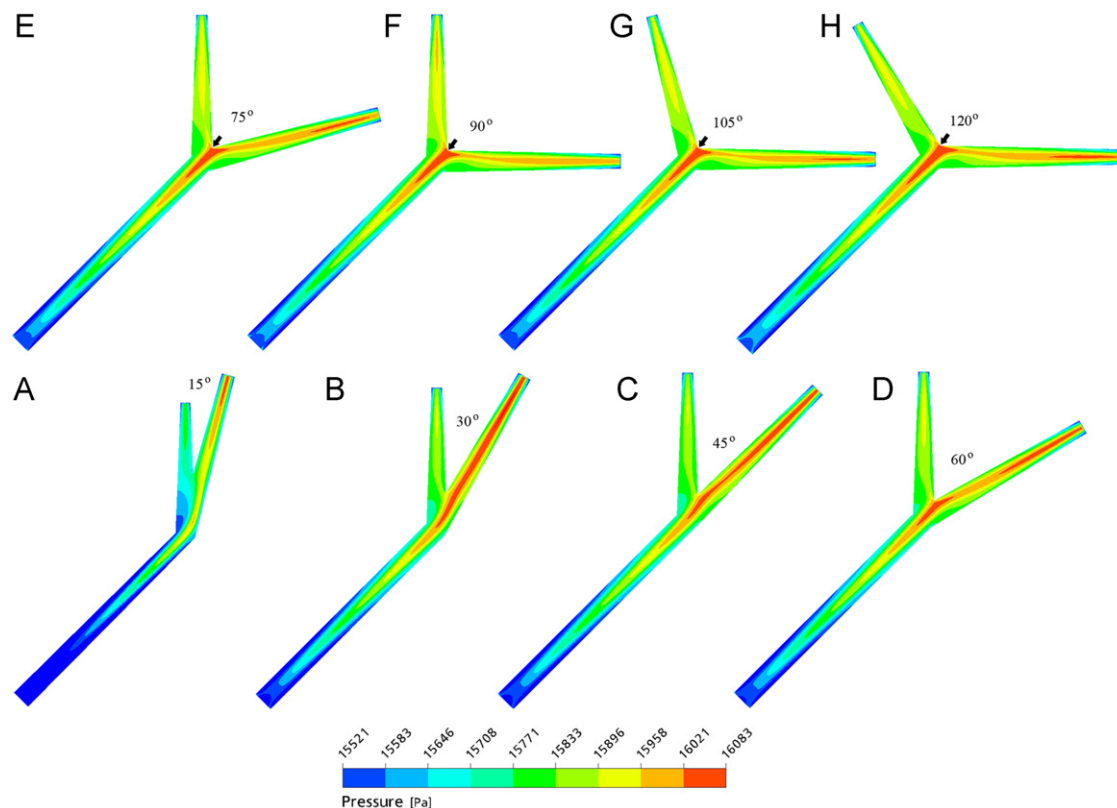


Fig. 7. Wall pressure observed with variable angles of the simulated left coronary artery models generated at peak systolic phase of 0.4 s. Arrows reveal the high wall pressure distributions at wide angulations and a 15° angulation displays the low wall pressure at coronary bifurcation.

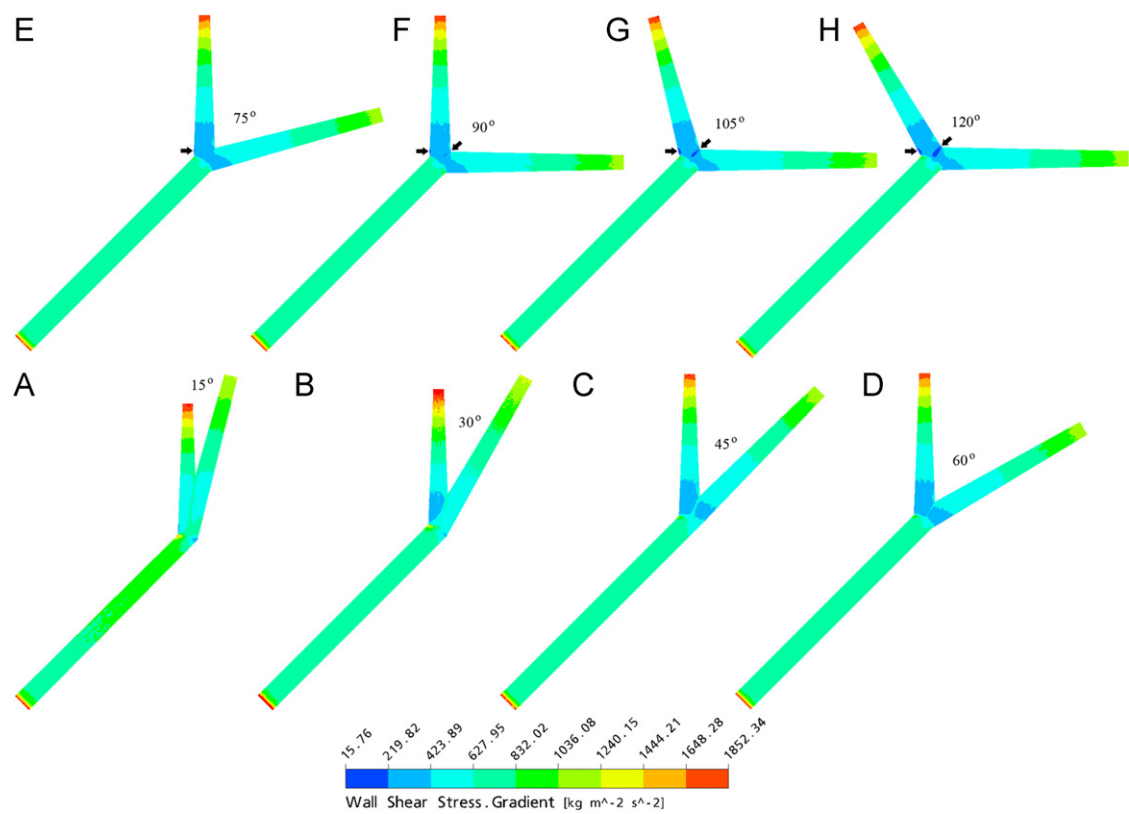


Fig. 8. Wall shear stress gradient observed with variable angles of the simulated left coronary artery models generated at peak systolic phase of 0.4 s. Arrows display the wall shear stress gradient distributions and a big region of the low magnitude present at a 120° angulation model.

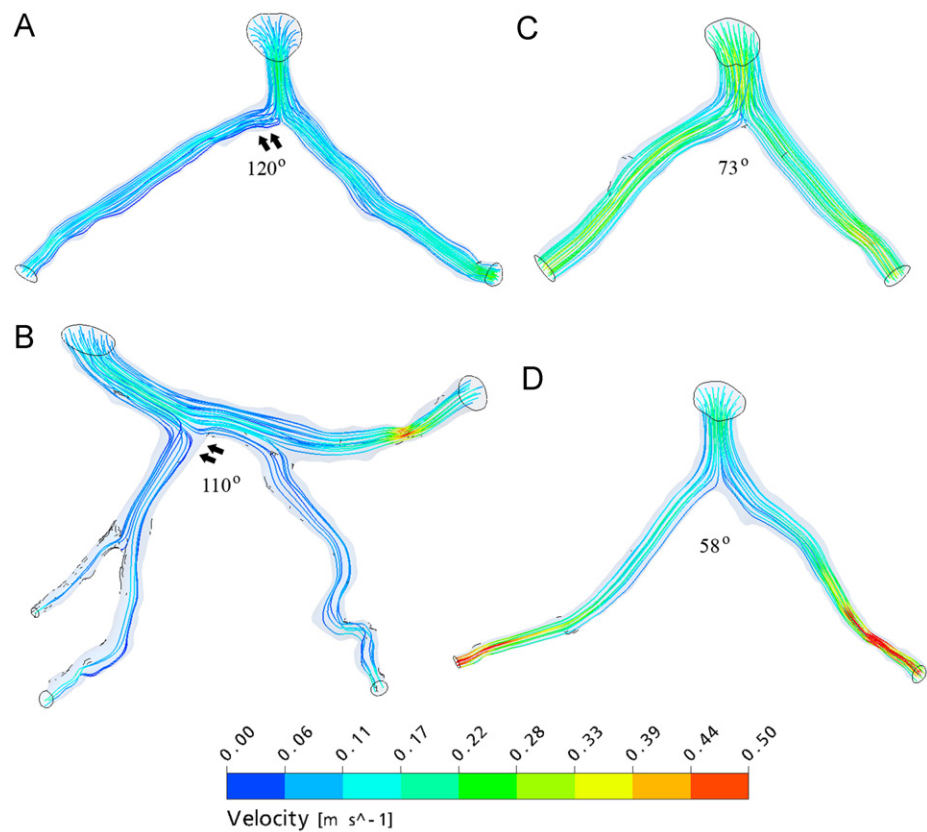


Fig. 9. Velocity observed with variable angles of the realistic left coronary artery models generated at peak systolic phase of 0.4 s. Double arrows show the big region of low flow at coronary bifurcations.

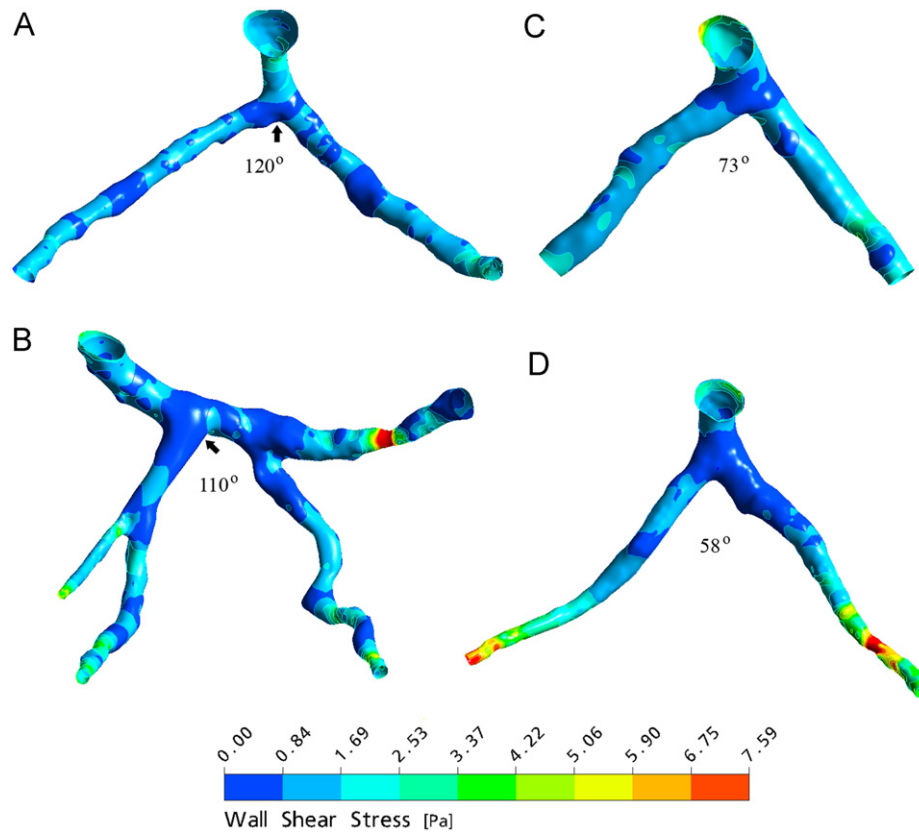


Fig. 10. Wall shear stress observed with variable angles of the realistic left coronary artery models generated at peak systolic phase of 0.4 s. Arrows refer to the low wall shear stress distributions at coronary bifurcations.

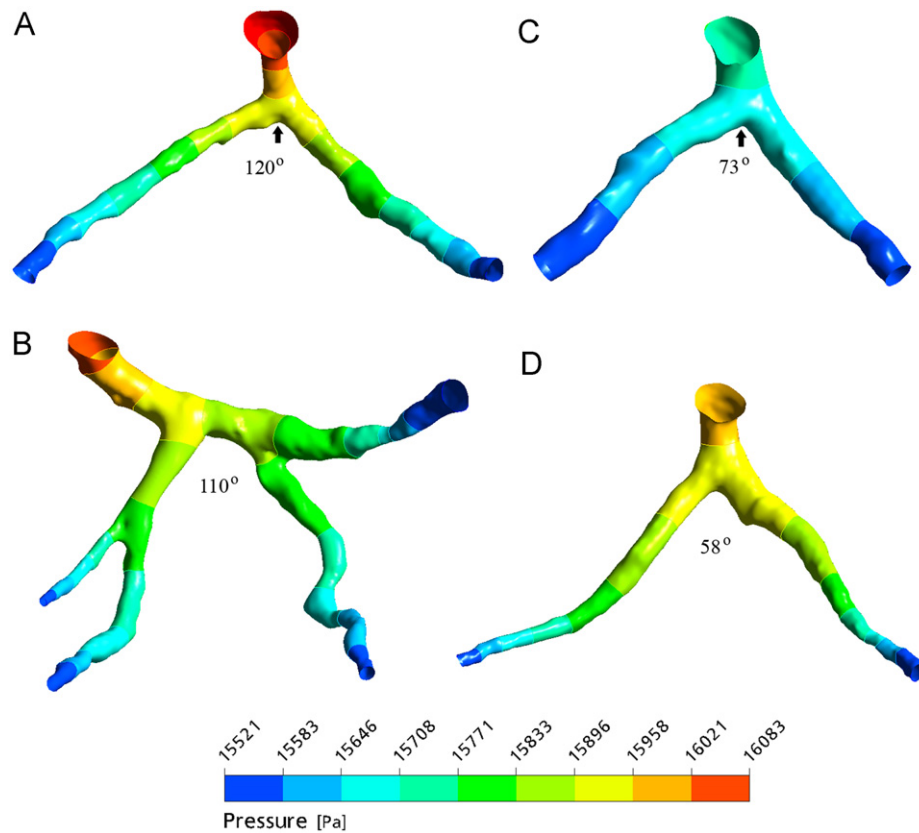


Fig. 11. Wall pressure observed with variable angles of the realistic left coronary artery models generated at peak systolic phase of 0.4 s. Arrows indicate the pressure distributions at coronary bifurcations and display higher wall pressure in a 120° angulation model than that of a 73° model.

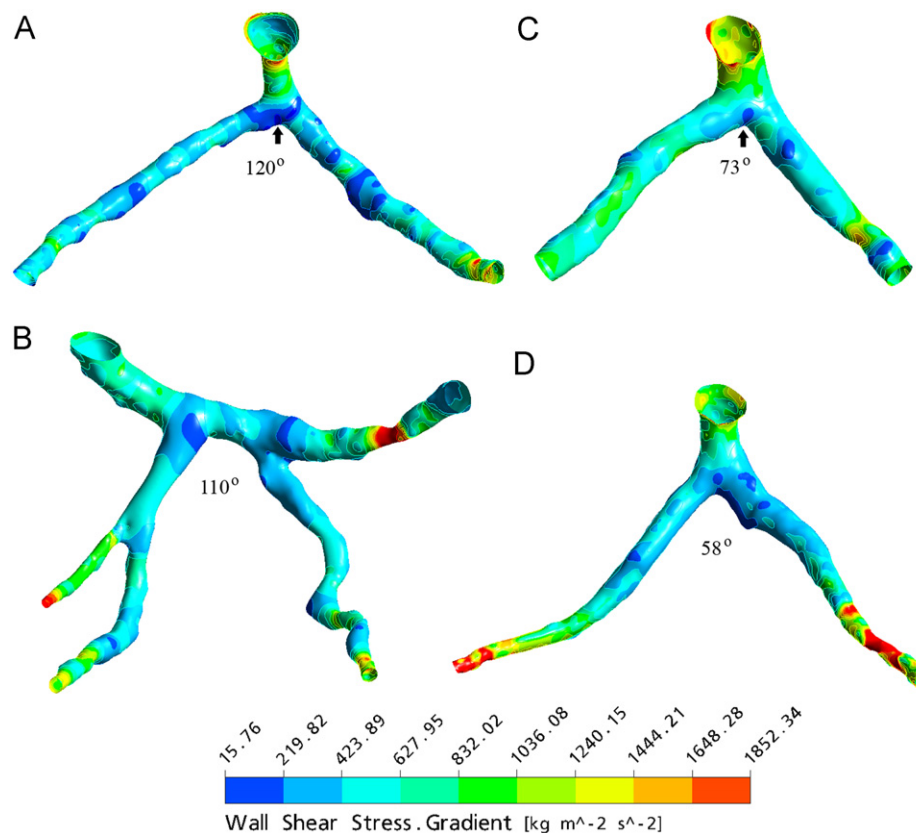


Fig. 12. Wall shear stress gradient observed with variable angles of the realistic left coronary artery models generated at peak systolic phase of 0.4 s. Arrows display the wall shear stress gradient distributions, with a large region of the low magnitude present in a 120° model and a small region in a 73° model.

4. Discussion

Our results based on simulated and realistic coronary models showed that there is a direct correlation between angulations of the left coronary artery and subsequent hemodynamic changes. Low wall shear stress and wall shear stress gradient were noticed in wide-angled models, and this indicates the potential risk of developing atherosclerosis at the left coronary bifurcation.

It is believed that local hemodynamic forces play an important role in the formation of atherosclerosis (Malek et al., 1999; Chien, 2007; Schroeder and Falk, 1995). Soulis et al. (2006) explored the change of WSS in the reconstructed left coronary artery and its branches with inclusion of coronary bifurcation. The hemodynamic analysis in their study showed that the atherosclerosis plaques frequently occurred in bifurcation regions where WSS was low. This is confirmed in our study, as a large region of low WSS was noticed at wide-angled models, indicating the tendency to induce atherosclerotic changes.

Early studies reported that atherosclerotic plaques tend to form at specific locations of the coronary artery such as the proximity branches, curvatures and bifurcations, where the flow separation occurred and WSS was low (Katritsis et al., 2007; Soulis et al., 2006; VanderLaan et al., 2004; Tarbell, 2010; Qi et al., 2008). Later reports further confirmed these early observations (Katritsis et al., 2007; Nordgaard et al., 2010). Katritsis et al. (2007) investigated the WSS oscillations based on the simulated artery bifurcation model comprising a straight tube, and their results showed that low wall shear stress occurred in the bifurcation locations. Nordgaard et al. (2010) in their recent report studied WSS in the remodeled left coronary artery and stated that low WSS was found in regions of low flow rate. Again, our analysis is consistent with these observations. Further to the

simulated models we included a number of models generated from patients' data with variable left coronary bifurcation angles, which is one of the advantages of the current study. Another advantage of our study is the direct comparison between two types of model, which showed consistent results. This indicates the additional value provided by this study.

In addition to the conventional CFD analysis, quantitative analysis of the impact of bifurcation angulations on hemodynamic flow was performed in this study by analyzing WSSG. The magnitude of wall shear stresses causes elongation and alignment of endothelial cells, while WSSG has direct effects on intercellular tension. The strong correlation between averaged low WSS and the localization of atherosclerotic lesions in arterial bifurcations has been well established (Katritsis et al., 2007; Soulis et al., 2006). However, WSS analysis topographically restricts the corresponding regions of low WSS at the vicinity of the coronary artery branches (Farmakis et al., 2004). Thus, low WSS regions appear to cover smaller surface area than the corresponding regions prone to developing atherosclerosis (Montenegro and Eggen, 1968). In contrast, low WSSG has been reported to clearly describe the regions where atherosclerosis prevails (Kleinstreuer et al., 2001). Hence, WSSG analysis seems to better depict these regions than WSS analysis does. Our analysis showed that the WSSG distribution tends to form a large area of low magnitude in wide-angled models, particularly at the region of bifurcation, while this was not apparent in narrow-angled models, as shown in Figs. 8 and 12. Consequently, the wide-angled bifurcations at left coronary artery may have a higher possibility to promote the atherosclerotic formation and progression than the narrow-angled bifurcations.

There are some limitations in our study that should be addressed. Firstly, the simulated and realistic left coronary

models were assumed to have a rigid wall rather than elastic wall; therefore, the simulation does not fully reflect the realistic physiological situation as coronary wall moves during cardiac cycles. Secondly no pathological changes such as presence of plaques or coronary stenosis were simulated in this study, since our focus was simply to investigate the relationship between angulation and hemodynamic changes. Thirdly the assumption of a Newtonian blood model has limitations on the biological effects of prolonged contact of blood flow with the cells of vascular wall, for example, platelet deposition (van Zanten et al., 1994) and leukocyte rolling (Sequeira et al., 2009). Additionally, a non-Newtonian blood model becomes important especially in low flow and low wall shear stress regions. However, previous studies have showed that the assumption of a Newtonian model is reasonable in this configuration (Johnston et al., 2006; Pedley, 1980). Fourthly, although cardiac CT has been increasingly used in the diagnosis of coronary artery disease with its improved diagnostic accuracy due to technological developments (Sun and Ng, 2010; Sun et al., 2008), the real CT patient data with representation of these coronary artery branches is limited for computational fluid dynamics analysis. Only four selected CT cases were included in this study, which limits our analysis. Although no significant coronary stenosis is demonstrated on these CT images, potential atherosclerotic changes in the coronary artery tree cannot be excluded given the fact that these patients are at high risk of developing atherosclerosis. However, the representative angles in these cases reflected the ranges from normal to abnormal coronary arteries thus, this limitation can be compensated for to some extent. Finally, although the geometry of simulated coronary models were based on patient's anatomical details, there are still inadequacies in the representation of realistic geometry, as most of the coronary arteries, especially at the left bifurcation, follow a curved as opposed to a straight path. Thus, future studies will use coronary models with a more realistic idealized geometry.

In conclusion, we studied the effect of various angulations of the left coronary artery on hemodynamics, based on simulated and realistic coronary models. There is a direct relationship between wide angulation in the left coronary bifurcation and hemodynamic changes such as disturbed flow and low wall shear stress and wall shear stress gradient, indicating the possible inducement of atherosclerosis. Further studies including patients with different risk factors or severity of coronary artery disease should be performed to verify our results.

Conflict of interest statement

None.

References

- Asakura, T., Karino, T., 1990. Flow patterns and spatial distribution of atherosclerotic lesions in human coronary arteries. *Circulation Research* 66, 1045–1066.
- Borghgi, A., Wood, N., Mohiaddin, R., Xu, X., 2008. Fluid–solid interaction simulation of flow and stress pattern in thoracoabdominal aneurysms: a patient-specific study. *Journal of Fluids and Structures* 24 (2), 270–280.
- Boutsianis, E., Dave, H., Frauenfelder, T., Poulikakos, D., Wildermuth, S., Turina, M., Ventikos, Y., Zund, G., 2004. Computational simulation of intracoronary flow based on real coronary geometry. *European Journal of Cardiothoracic Surgery* 26, 248–256.
- Chien, S., 2007. Mechanotransduction and endothelial cell homeostasis: the wisdom of the cell. *American Journal of Physiology—Heart and Circulatory Physiology* 292 (3), H1209–H1224.
- Conner, L.A., 1994. Mechanisms leading to myocardial infarction: insights from studies of vascular biology. *Circulation* 90, 2126–2146.
- Farmakis, T.M., Soulis, J.V., Giannoglou, G.D., Zioupos, G.J., Louridas, G.E., 2004. Wall shear stress gradient topography in the normal left coronary arterial tree: possible implications for atherogenesis. *Current Medical Research and Opinion* 20, 587–596.
- Frauenfelder, T., Lotfey, M., Boehm, T., Wildermuth, S., 2006. Computational fluid dynamics: hemodynamic changes in abdominal aortic aneurysm after stent-graft implantation. *Cardiovascular and Interventional Radiology* 29 (4), 613–623.
- He, X., Ku, D.N., 1995. Flow in T-bifurcations: effect of the sharpness of the flow divider. *Biorheology* 32, 447–458.
- Johnston, B., Johnston, P., Corney, S., Kilpatrick, D., 2006. Non-Newtonian blood flow in human right coronary arteries: transient simulations. *Journal of Biomechanics* 39 (6), 1116–1128.
- Johnston, B., Johnston, P., Corney, S., Kilpatrick, D., 2004. Non-Newtonian blood flow in human right coronary arteries: steady state simulations. *Journal of Biomechanics* 37 (5), 709–720.
- Katritsis, D., Kaiktsis, L., Chaniotis, A., Pantos, J., Efstathiopoulos, E.P., Marmarelis, V., 2007. Wall shear stress: theoretical considerations and methods of measurement. *Progress in Cardiovascular Diseases* 49 (5), 307–329.
- Kleinstreuer, C., Hyun, S., Buchanan, J.R., Longest, P.W., Archie, J.P., Truskey, J.P., 2001. Hemodynamic parameters and early intimal thickening in branching blood vessels. *Critical Reviews in Biomedical Engineering* 29 (1), 1–64.
- LaDisa, J.F., Olsan, L.E., Guler, I., Hettrick, D.A., Kersten, J.R., Warltier, D.C., Pagel, P.S., 2004. Circumferential vascular deformation after stent implantation alters wall shear stress evaluated with time-dependent 3D computational fluid dynamics models. *Journal of Applied Physiology* 98, 947–957.
- Lehoux, S., 2006. Redox signalling in vascular responses to shear and stretch. *Cardiovascular Research* 71 (2), 269–279.
- Lei, M., Giddens, D.P., Jones, S.A., Loth, F., Bassiouny, H., 2001. Pulsatile flow in an end-to-side vascular graft model: comparison of computations with experimental data. *Journal of Biomechanical Engineering* 123, 80–87.
- Lei, M., Kleinstreuer, C., Truskey, G.A., 1996. A focal stress gradient-dependent mass transfer mechanism for atherogenesis in branching arteries. *Medical Engineering and Physics* 18 (4), 326–332.
- Lim, M.J., Kern, M.J., 2005. Utility of coronary physiologic hemodynamics for bifurcation, aorto-ostial, and ostial branch stenoses to guide treatment decisions. *Catheterization and Cardiovascular Interventions* 65 (4), 461–468.
- Lou, Z., Yang, W.J., 1993. A computer simulation of the non-Newtonian blood flow at the aortic bifurcation. *Journal of Biomechanics* 26, 37–49.
- Malek, A.M., Alper, S.L., Izumo, S., 1999. Hemodynamic shear stress and its role in atherosclerosis. *Journal of American Medical Association* 282 (21), 2035–2042.
- Milnor, W.R., 1989. *Hemodynamics*. Williams & Wilkins, Baltimore.
- Montenegro, M.R., Eggen, D.A., 1968. Topography of atherosclerosis in the coronary arteries. *Laboratory Investigation* 18, 586–593.
- Nichols, W.W., O'Rourke, M.F., 2005. *McDonald's Blood Flow in Arteries*, fifth ed. Hodder Arnold, London 326–327.
- Nordgaard, H., Swillens, A., Nordhaug, D., Kirkeby-Garstad, I., Loo, D., Vitale, N., Segers, P., Haaverstad, R., Lovstakken, L., 2010. Impact of competitive flow on wall shear stress in coronary surgery: computational fluid dynamics of a LIMA–LAD model. *Cardiovascular Research* 88 (3), 512–519.
- Ojha, M., 1993. Spatial and temporal variations of wall shear stress within an end-to-side arterial anastomosis model. *Journal of Biomechanics* 26, 1377–1388.
- Pedley, T.J., 1980. *The Fluid Mechanics of Large Blood Vessels*. Cambridge university press, Cambridge, pp. 30–31.
- Pfleiderer, T., Ludwig, J., Ropers, D., Daniel, W.G., Achenbach, S., 2006. Measurement of coronary artery bifurcation angles by multidetector computed tomography. *Investigative Radiology* 41, 793–798.
- Qi, Y.X., Qu, M.J., Long, D.K., Liu, B., Yao, Q.P., Chien, S., Jiang, Z.L., 2008. Rho-GDP dissociation inhibitor alpha down regulated by low shear stress promotes vascular smooth muscle cell migration and apoptosis: a proteomic analysis. *Cardiovascular Research* 80 (1), 114–122.
- Reig, J., Petit, M., 2004. Main trunk of the left coronary artery: anatomic study of the parameters of clinical interest. *Clinical Anatomy* 17, 6–13.
- Sabbah, H.N., Khaja, F., Hawkins, E.T., Brymer, J.F., McFarland, T.M., van der Bel-Kahn, J., Doerger, P.T., Stein, P.D., 1986. Relation of atherosclerosis to arterial wall shear in the left anterior descending coronary of man. *American Heart Journal* 112 (3), 453–458.
- Schroeder, A., Falk, E., 1995. Vulnerable and dangerous coronary plaques. *Atherosclerosis (Suppl.)*, S141–S149.
- Sequeira, A., Artoli, A.M., Silva-Herdade, A.S., Saldanha, C., 2009. Leukocytes dynamics in microcirculation under shear-thinning blood flow. *Computers and Mathematics with Applications* 58, 1035–1044.
- Shanmugavelayudam, S.K., Rubenstein, D., Yin, W., 2010. Effect of geometrical assumptions on numerical modeling of coronary blood flow under normal and disease conditions. *Journal of Biomechanical Engineering* 132 (6), 061004.
- Smith, S.W., 1997. *The scientist and engineer's guide to digital signal processing*. California Technical Publishing, California, pp. 255–256.
- Soulis, J.V., Farmakis, T.M., Giannoglou, G.D., Louridas, G.E., 2006. Wall shear stress in normal left coronary artery tree. *Journal of Biomechanics* 39 (4), 742–749.
- Sun, Z., Chaichana, T., 2010. Fenestrated stent graft repair of abdominal aortic aneurysm: hemodynamic analysis of the effect of fenestrated stents on the renal arteries. *Korean Journal of Radiology* 11 (1), 95–106.
- Sun, Z., Chaichana, T., 2009. Investigation of the hemodynamic effect of stent wires on renal arteries in patients with abdominal aortic aneurysms treated with suprarenal stent-grafts. *Cardiovascular and Interventional Radiology* 32 (4), 647–657.
- Sun, Z., Winder, R.J., Kelly, B.E., Ellis, P.K., Kennedy, P.T., Hirst, D.G., 2004. Diagnostic value of CT virtual intravascular endoscopy in aortic stent grafting. *Journal of Endovascular Therapy* 11 (1), 13–25.

- Sun, Z., Winder, R.J., Kelly, B.E., Ellis, P.K., Hirst, D.G., 2003. CT virtual intravascular endoscopy of abdominal aortic aneurysms treated with suprarenal endovascular stent grafting. *Abdominal Imaging* 28 (4), 580–587.
- Sun, Z., Ng, K.H., 2010. Multislice CT angiography in cardiac imaging. Part II: clinical applications in coronary artery disease. *Singapore Medical Journal* 51 (4), 282–289.
- Sun, Z., Lin, C.H., Davidson, R., Dong, C., Liao, Y., 2008. Diagnostic value of 64-slice CT angiography in coronary artery disease: a systematic review. *European Journal of Radiology* 67, 78–84.
- Tarbell, J.M., 2010. Shear stress and the endothelial transport barrier. *Cardiovascular Research* 87 (2), 320–330.
- VanderLaan, P.A., Reardon, C.A., Getz, G.S., 2004. Site specificity of atherosclerosis: site-selective responses to atherosclerotic modulators. *Arteriosclerosis Thrombosis and Vascular Biology* 24, 12–22.
- van Zanten, G.H., de Graaf, S., Slootweg, P.J., Heijnen, H.F., Connolly, T.M., de Groot, P.G., Sixma, J.J., 1994. Increased platelet deposition on atherosclerotic coronary arteries. *Journal of Clinical Investigation* 93 (2), 615–632.
- Wellnhofer, E., Osman, J., Kertzscher, U., Affeld, K., Fleck, E., Goubergrits, L., 2010. Flow simulation studies in coronary arteries—impact of side-branches. *Atherosclerosis* 213 (2), 475–481.
- White, C.R., Haidekker, M., Bao, X., Frangos, J.A., 2001. Temporal gradients in shear, but not spatial gradients, stimulate endothelial cell proliferation. *Circulation* 103, 250–2513.
- World medical association declaration of Helsinki, 1997. Recommendations guiding physicians in biomedical research involving human subjects. *Cardiovascular Research* 35, 2–3.
- Zarins, C.K., Giddens, D.P., Bharadvaj, B.K., Sottiurai, V.S., Mabon, R.F., Glagov, S., 1983. Carotid bifurcation atherosclerosis. Quantitative correlation of plaque localization with flow velocity profiles and wall shear stress. *Circulation Research* 53, 502–514.
- Zheng, Y., Fujioka, H., Grotberg, J.C., Grotberg, J.B., 2006. Effects of inertia and gravity on liquid plug splitting at a bifurcation. *Journal of Biomechanical Engineering* 128, 707–716.